ISSN: 2319-5967
ISO 9001:2008 Certified
International Journal of Engineering Science and Innovative Technology (IJESIT)
Volume 4, Issue 3, May 2015

# Simulation of the Metal and Ceramic Powders Densification Process by Hot Isostatic Pressing

Locif REDOUANI [1], Smail BOUDRAHEM [2]
[1] Physicochemical of Materials Laboratory, Faculty of Sciences and Technology, Chadli Bendjedid University, El-Tarf 36000, Algeria
[2] Laboratory of Technology of Materials and Engineering of the Processes, Faculty of Technology, University Abderahman Mira, Bejaia 06000, Algeria

***Abstract*— Densification by hot isostatic pressing (HIP) of powders is very difficult to model. The HIP process involves several mechanisms of deformation and transport of matter difficult to quantify. HIP densification modeling is investigated in order to improve the agreement between experimental and simulation data. A simulation procedure is developed on the basis of micromechanical models. Numerical simulation of the HIP process assesses to the instantaneous relative density D of tablets. Diagrams densification of alumina, nickel-base super alloy and tool steel powders have been established showing the variation of relative density D as function of the pressure or temperature for the given time of treatment. The results show that the theoretical predictions are in good agreement with the experimental data.***

***Index terms*— Densification mechanisms, Hot Isostatic pressing, micromechanical approach, relative density.**

## I. INTRODUCTION

Hot isostatic pressing (HIP) is a powerful method for obtaining, using powders, mechanical parts directly to their final dimensions and the development of materials with compositions and microstructures infinitely varied. When a powder is heated and simultaneously submitted to high pressure, not only mechanisms occurring in pressure less sintering, such as lattice or boundary diffusion, are enhanced, but new mechanisms are activated which may become dominant. Indeed, when pressure is combined with temperature, it induces plastic yielding, power low creep or diffusional creep in the powder compact. Numerous models [1]-[3] have been proposed for each of these elementary mechanisms of densification. The overall densification rate is calculated in summing the different contributions. This kind of approach provides the basis for computing HIPing diagrams which allows the identification of the dominant mechanism of densification and the construction of isochrones curves which indicate the density of samples compacted at different pressures (or temperature) for a given time. Such HIPing diagrams are destined for industrial practices to determine the most efficient combination of process variables leading to the desired density with the desired microstructure. Unfortunately, an important disagreement is often observed between simulation predictions and experiments data. It is true that the extreme complexity of the stack structure of the powders on the one hand, and the diversity of mechanisms governing the densification, secondly, are difficult to take into account in the simulations. Finally, model validation is fraught with difficulties which are in experimental order due to randomness of grain stacks and polydispersity of powders. For all these reasons, process optimization HIP requires, even today, to develop new specific studies to improve the reliability of the models. It's in this context that the work is presented in this paper.

In order to overcome the difficulties related to the use of stacks of irregular structures, aggregates of powders is equated with random dense packing (RDP) of spherical particles of the same size. The use of this model allows us to express the coordination number of stacks of powder depending on the instantaneous relative density *D*. It then becomes easy to trace the expression of the mean effective pressure exerted on the contacts that form between the powder particles. The effective pressure is used to evaluate the contributions of the mechanisms of densification of powder aggregates.

It is assumed that the densification is the cumulative result of several mechanisms acting in parallel: the plastic yielding, power law creep, material flows associated with diffusions from the grain boundaries and Nabarro-Herring and Coble creep.

On these theoretical foundations, we have developed computing procedures to simulate HIP cycles of several powders. The theoretical predictions are compared with experimental measurements found in literature.

ISSN: 2319-5967
ISO 9001:2008 Certified
International Journal of Engineering Science and Innovative Technology (IJESIT)
Volume 4, Issue 3, May 2015

## II. PARAMETERS OF DENSE RANDOM PACKING

The used micromechanical approach left from a representation of the porous medium by a random dense packing (RDP) of spherical particles of the same radius *R*. This allows expressing the coordination number *Z*, the average area *a* of contact between the particles and the effective pressure $P_{eff}$ based on the instantaneous relative density *D*. The densification of a RDP by hot isostatic pressing is then simulated by increasing the radius of spherical particles about their centers that are stationary. The new particle radius is estimated by:

$$R' = R\left(D/D_0\right)^{1/3} \tag{1}$$

The radius particle growth generates a volume of excess material which is distributed on the free surfaces of the particles. These results increase in the number of contacts Z which, according to Arzt [4], obeys to the law:

$$Z = Z_0 + C\left[\left(R'/R\right) - 1\right] \tag{2}$$

The compression of a porous medium generates a stress concentration at the contacts between particles as porous cavities do not allow the transmission of these constraints. The mean effective pressure $P_{eff}$ exerted on the contacts is then amplified. It can be estimated from [5]:

$$P_{eff} = \left(4\pi R^2/Za\right)P \tag{3}$$

The morphological changes that occur within the tablet during the densification process by HIP are described considering that are resulting from a succession of two stages.

In stage I, the relative density is between 0.64 and 0.92, the pores are interconnected and the particles remain separate [6]. The densification which occurs in this stage is accompanied by a net increase coordination and expansion of contact surfaces that form between the particles.

The final densification stage (stage II) is characterized by closed porosity and a spherical shape. Densification occurs through progressive elimination of porosity [7], [8].

### *A. Stage I*

During this stage the contacts between spherical particles increase in size and number. Densification occurs by deformation and matter transfer from contact points to free neck surfaces which form between particles.

Equations corresponding to the various contributions are calculated using the simplified expression of the average coordination number obtained by Helle and his collaborators [3], namely:

$$Z = 12D \tag{4}$$

The average area of circular contacts that form between the spherical particles of the EAD in the first stage of densification is evaluated by:

$$a = \left(2\pi/3\right)\left[\left(D - D_0\right)/D_0\right]R^2 \tag{5}$$

As for the average radius of the contact surface between the particles, it is given by:

$$x = \left(a/\pi\right)^{1/2} = \left\{\left(2/3\right)\left[\left(D - D_0\right)/D_0\right]\right\}^{1/2} R \tag{6}$$

Replacing *Z* and *a* by their respective expressions (4) and (5) in (3), we obtain the expression of the effective pressure $P_{eff}$, namely:

$$P_{eff} = \left\{D_0/\left[2D\left(D - D_0\right)\right]\right\}P \tag{7}$$

### *B. Stage II*

During the final stage of densification, it is considered that the porous phase is in the form of a fine dispersion of spherical pores. Densification then continues by eliminating porosity dating back to the tablet surface without significant change in the coordination number. It is estimated, therefore, that during this stage *Z* remains constant and equal to 12.

The model system that is most appropriate to describe the morphology of the particles during the final stage of densification is a dodecahedron. This geometry contains 12 pentagonal facets, each one corresponds to a contact, and its vertices are occupied by the spherical pores. This configuration enables to evaluate easily the radius of the spherical pores $r_p$ and the average contact area *a* as a function of *D* and *R*. The calculations lead to the following expressions [5]:

$$r_p = R\left[\left(1 - D\right)/5D\right]^{1/3} \tag{8}$$

$$a = \left(\pi R^2/3\right)\left\{1 - 5\left[\left(1 - D\right)/5D\right]^{1/3}\right\} \tag{9}$$

Effective pressure can thus be evaluated by:

ISSN: 2319-5967
ISO 9001:2008 Certified
International Journal of Engineering Science and Innovative Technology (IJESIT)
Volume 4, Issue 3, May 2015

$$P_{eff} = \left\{1/1-5\left[(1-D)/5D\right]^{1/3}\right\}P \quad (10)$$

This expression shows that the effective pressure tends to the external hydrostatic pressure when the densification is complete ($D$=1).

## III. DENSIFICATION MECHANISMS SIMULATION

The various mechanisms that operate in the HIP processes are analyzed within the particles and their closest neighbors. It is assumed that the densification is the cumulative result of several mechanisms acting in parallel: the plastic yielding, power law creep, Nabarro-Herring and Coble creep and material flows associated with lattice and joints grains diffusions.

### *A. Plastic yielding*

Early in the process of densification by hot isostatic pressing, contacts between particles are very small (points). The applied pressure generates very high local stresses, thereby causing plastic yielding of the contact between the particles.

It is assumed that the plastic yielding takes place when the effective pressure on contact is greater than or equal to the limit value $3\sigma_y$ ($\sigma_y$ is the yield stress of the base material powders). The limit pressure of plastic yielding is given by:

$$P_{\lim} = P_{eff} = 3\sigma_y \quad (11)$$

Combining (7) and (11), and after calculation, it leads to the expression of the relative density $D_y$ reached in the tablet after plastic yielding of contacts between the particles, namely:

$$D_y = (D_0/2)\left\{1+\left[1+(2/3D_0)(P/\sigma_y)\right]^{1/2}\right\} \quad (12)$$

### *B. Power law creep*

Expanding contacts by plastic yielding lead to a sharp decrease in effective pressure. Plastic yielding of the contact can't take place. Densification continues then by the thermally activated mechanisms, such as creep. This phenomenon is considered to be a slow and continuous deformation in time.

When the deformation increases continuously with time and that the creep rate increases exponentially with temperature, it is governed by a constitutive law of the form:

$$\dot{\varepsilon} = A\sigma^n \quad (13)$$

The constant $A$ is given by:

$$A = \dot{\varepsilon}_0/\sigma_0^n = (A'\,b\,D_v)/(kT\mu^{n-1}) \quad (14)$$

The contribution of the power law creep in the first stage of densification is assessed using the geometric model of nested spherical particles and the laws of Hertz for circular contacts [5]. The resulting expression is:

$$\Delta D = 2A(D_0/D)^{1/3}\left[D(D-D_0)/D_0\right]^{1-n}(P/6)^n\,\Delta t \quad (15)$$

In stage II, we addressed the problem by using the geometric model of Wilkinson and Ashby [9]. It is considered that the pores are surrounded by a spherical shell of material subjected to the hydrostatic pressure $P$. The resulting expression is:

$$\Delta D = A(3/2)\left\{D(1-D)/\left[1-(1-D)^{1/n}\right]^n\right\}(3P/2n)^n\,\Delta t \quad (16)$$

### *C. Diffusion mechanisms*

Diffusion mechanisms that contribute to densification are those which cause a mass transfer contact surfaces (joints) which form between the particles to the free surfaces of the particles (porosity). Two mechanisms are included. There are grain boundary diffusion with material flow from the joint and through this one and lattice diffusion from the joint but through the atomic lattice.

In stage I, the expressions of grain-boundary diffusion and lattice diffusion mechanisms contributions are respectively given by:

$$\Delta D = 72(\delta D_b\Omega/kTR^3)\left[(D_0^{1/3}D^{1/3})/\left(\left[(D/D_0)^{1/3}-1\right]\left\{2Z_0+C\left[(D/D_0)^{1/3}-1\right]\right\}\right)\right]\left[P/(D-D_0)\right]\Delta t \quad (17)$$

$$\Delta D = 59(D_v\Omega/kTR^2)\left[(D_0^{1/3}D^{1/3})/\left(\left[(D/D_0)^{1/3}-1\right]\left\{2Z_0+C\left[(D/D_0)^{1/3}-1\right]\right\}\right)\right]\left[P/(D-D_0)^{1/2}\right]\Delta t \quad (18)$$

In stage II, they are respectively evaluated by:

$$\Delta D = 27(\delta D_b\Omega/kTR^3)\left(D^2/\left\{1-5\left[(1-D)/5D\right]^{1/3}\right\}\right)P\,\Delta t \quad (19)$$

ISSN: 2319-5967
ISO 9001:2008 Certified
International Journal of Engineering Science and Innovative Technology (IJESIT)
Volume 4, Issue 3, May 2015

$$\Delta D = 15\left(D_v \Omega / kTR^2\right)\left(D^2\left[(1-D)/5D\right]^{1/3} / \left\{1-5\left[(1-D)/5D\right]^{1/3}\right\}\right)P\Delta t \quad (20)$$

### *D. Nabarro-Herring/Coble creep*

The basic equation which describes the flow of material by diffusion (Nabarro-Herring/Coble creep) from the interior of the powder particles to the pores is given by:

$$\dot{\varepsilon} = \left(12\Omega / kT\bar{G}^2\right)\left[D_v + \left(\pi\delta D_b / \bar{G}\right)\right]\sigma \quad (21)$$

The number 12 corresponds to the number of nearest neighbors of the reference particle.

It is obvious that this type of densification mechanism is taken into account only in the case where $\bar{G}$ is very small compared to the radius *R* of the particles.

Contributions associated with stage I and stage II are respectively given by:

$$\Delta D = 4\left(\Omega / kT\bar{G}^2\right)\left(D_0 / D\right)^{1/3}\left[D_v + \left(\pi\delta D_b / \bar{G}\right)\right]P\,\Delta t \quad (22)$$

$$\Delta D = 27\left(\Omega / kT\bar{G}^2\right)(1-D)\left[D_v + \left(\pi\delta D_b / \bar{G}\right)\right]P\,\Delta t \quad (23)$$

## IV. DENSIFICATION MAPS

The used simulation method consists to divide the duration of the level (processing time) in a large number of small intervals of time $\Delta t$ equal to one second.

The relative density $D_y$ obtained after plastic yielding is calculated at the beginning of the level when the treatment pressure and temperature are highest. If densification has not reached the second stage ($D$<0.92) or not complete ($D$<1), the time t is incremented by one second, the contributions of the other mechanisms, time-dependent, are calculated by taking into account the value of the relative density obtained.

Contributions calculated at each increment are added to the previous until the final density is reached or the processing time is exhausted.

Once the final relative density is obtained, the procedure is repeated by varying the temperature for a given pressure or vice versa.

HIP densification maps of alumina powders, nickel-based super alloy and tool steel were established by increasing the relative density as a function of temperature and different treatment times for a given pressure. The separation of dominant mechanisms is carried out by comparison of the different contributions calculated based on the density achieved in the tablet during the densification process. The calculations make use of the physical constants of the basic materials powders studied given in table 1.

**Table 1. Values of the used constants in the densification simulations of alumina, tool steel and nickel-based super alloy powders found in literature [1], [3], [10], [11].**

| Constants | Alumina | Tool steel | Superalloy |
|---|---|---|---|
| $R$(m) | 1,25 x $10^{-6}$ | 50 x $10^{-6}$ | 50 x $10^{-6}$ |
| $\bar{G}$(m) | / | $10^{-5}$ | $10^{-5}$ |
| $T_m$(K) | 2320 | 1680 | 1673 |
| $\mu_0$ (MPa) | 1,55 x $10^5$ | 8,1 x $10^4$ | 8,3 x $10^4$ |
| β | -0,35 | -0,85 | -0,5 |
| $\sigma_{y0}$ (MPa) | 2100 | 200 | 180 |
| α | -0,35 | -0,85 | -0,5 |
| Ω ($m^3$) | 4,25 x $10^{-29}$ | 1,21 x $10^{-29}$ | 1,1 x $10^{-29}$ |
| $D_{0v}$($m^2s^{-1}$) | 2,8 x $10^{-10}$ | 3,7 x $10^{-5}$ | 1,6 x $10^{-4}$ |
| $Q_v$(KJ $mole^{-1}$) | 477 | 280 | 285 |
| $\delta D_{0b}$($m^3s^{-1}$) | 8,6 x $10^{-10}$ | 2 x $10^{-13}$ | 2,8 x $10^{-15}$ |
| $Q_b$(KJ $mole^{-1}$) | 419 | 167 | 115 |
| n | 3 | 7,5 | 4,6 |
| $A'$ | 3,38 | 1,5x $10^{12}$ | 1,22x $10^5$ |
| $b$(m) | 4,76 x $10^{-10}$ | 2,58 x $10^{-10}$ | 2,5 x $10^{-10}$ |

ISSN: 2319-5967
ISO 9001:2008 Certified
International Journal of Engineering Science and Innovative Technology (IJESIT)
Volume 4, Issue 3, May 2015

Examples of alumina, super alloy and steel densification maps are represented by the graphs of figures 1, 2 and 3.

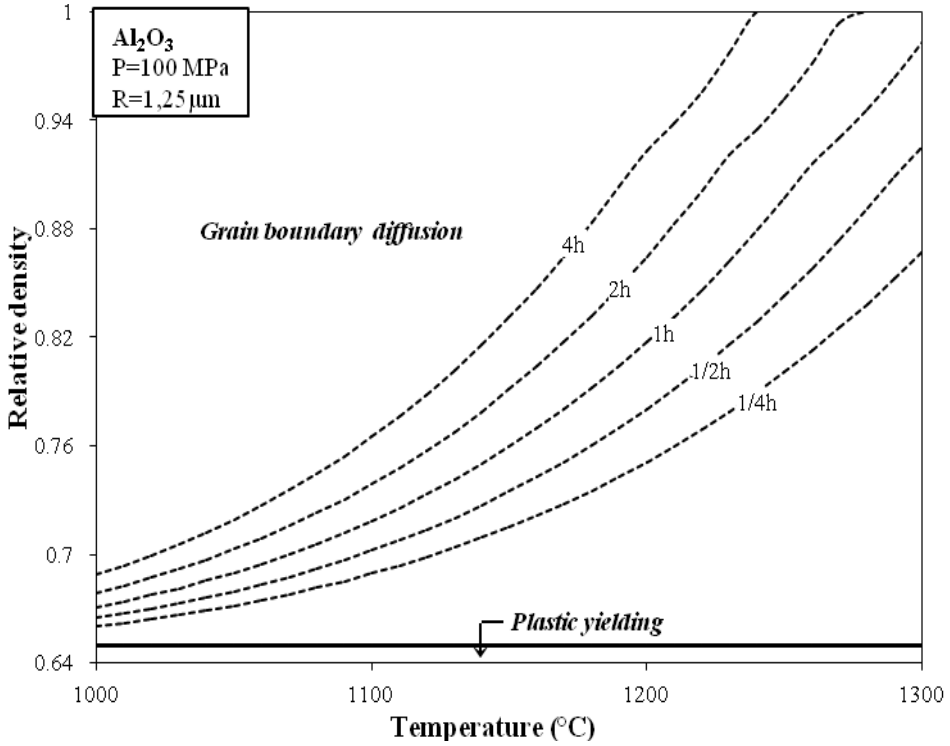


**Fig.1. HIP densification map of alumina powder subjected to a pressure of 100 MPa.**

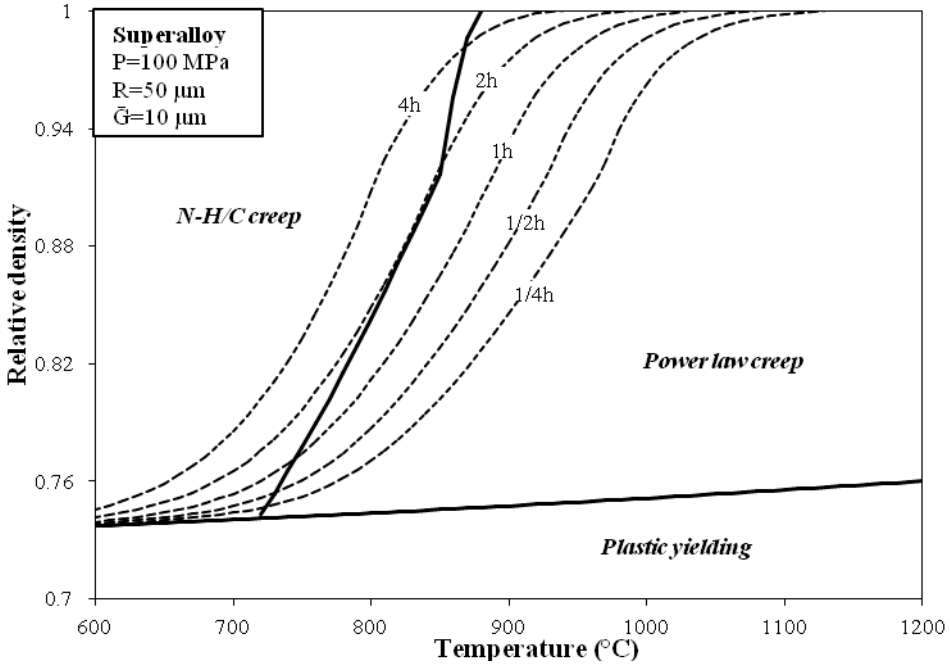


**Fig.2. HIP densification map of nickel-based super alloy powder subjected to a pressure of 100 MPa.**

ISSN: 2319-5967
ISO 9001:2008 Certified
International Journal of Engineering Science and Innovative Technology (IJESIT)
Volume 4, Issue 3, May 2015

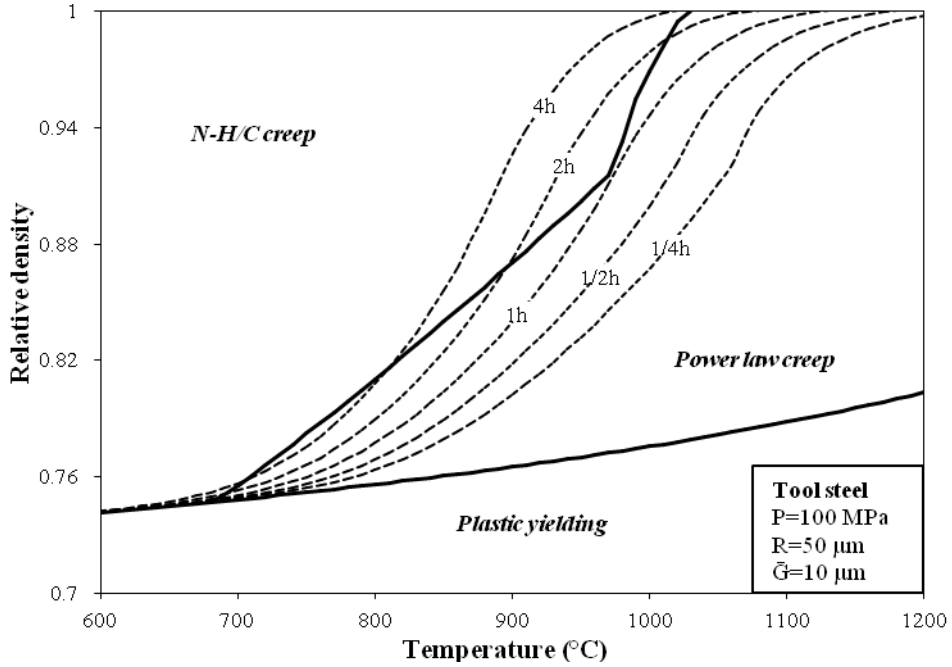


**Fig.3. HIP densification map of tool steel powder subjected to a pressure of 100 MPa.**

## V. VALIDATION OF RESULTS

Within the context of analysis of the numerical simulations results of hot isostatic pressing process of metal and ceramic powders, we made comparisons with several sets of experimental data found in literature [1], [3], [6]. The comparisons reveal, in most cases studied, a good agreement between the simulation predictions and experimental data (Fig.4, Fig.5 and Fig.6).

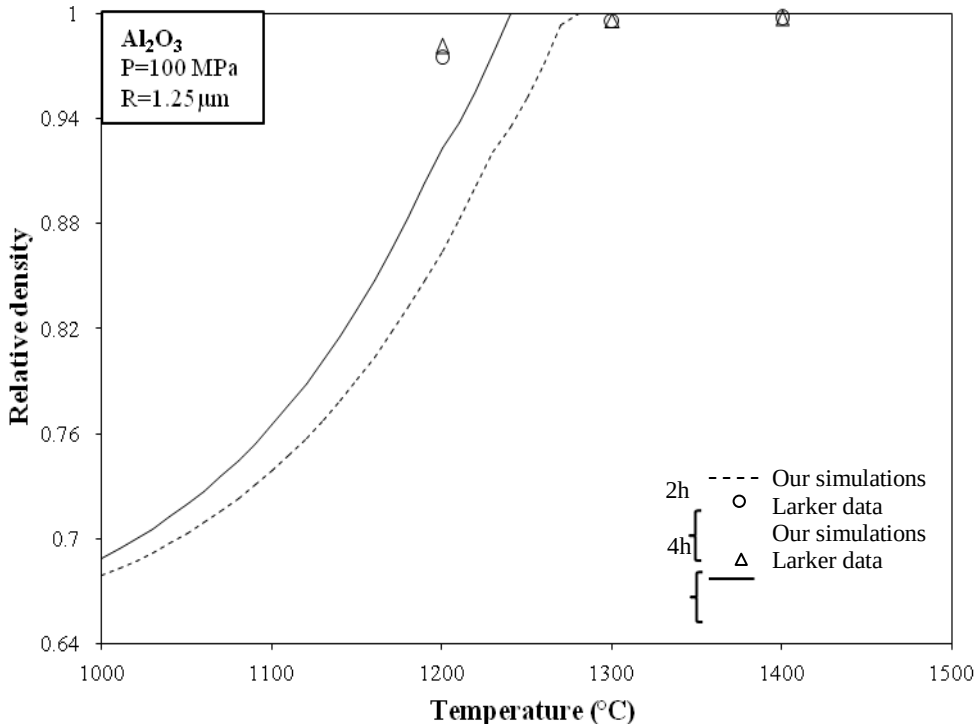


**Fig.4. Comparison between the relative densities given by the simulation predictions and experimental results of Larker [1], [3] relating to alumina powder subjected to 100 MPa for periods of 2 h and 4 h.**

ISSN: 2319-5967
ISO 9001:2008 Certified
International Journal of Engineering Science and Innovative Technology (IJESIT)
Volume 4, Issue 3, May 2015

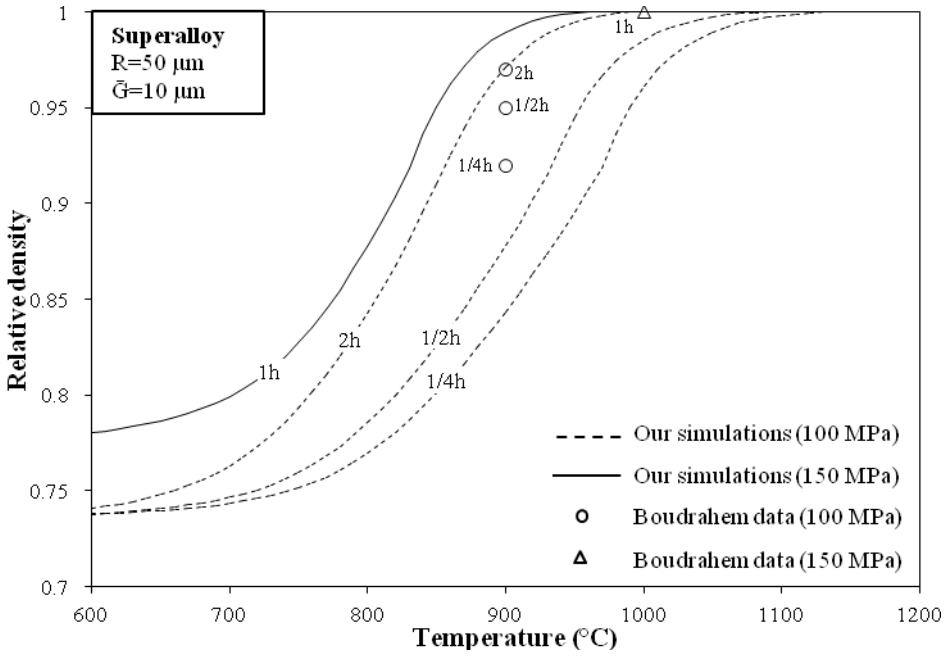


**Fig.5. Comparison between the relative densities given by the simulation predictions and experimental results of Boudrahem and Grosbras [6] relating to nickel-based super alloy powder.**

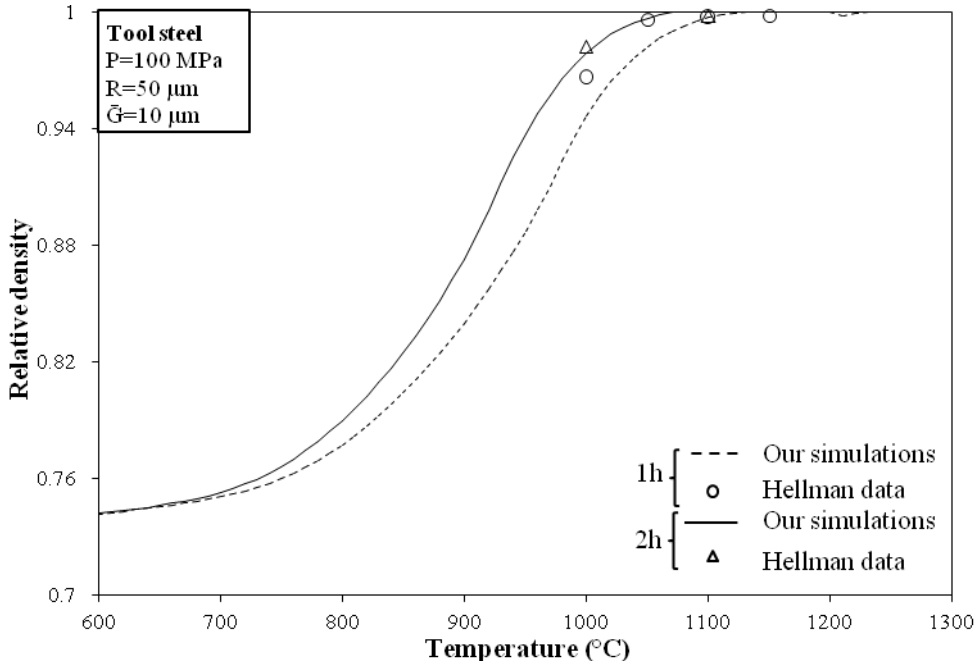


**Fig.6. Comparison between the relative densities given by the simulation predictions and experimental results of Hellman [1], [3] corresponding to tool steel powder subjected to 100 MPa for periods of 1 h and 2 h.**

## VI. RESULTS AND DISCUSSION

Densification maps of alumina, nickel-base super alloy, and tool steel powders have been established showing the variation of relative density *D* as function of the temperature for given pressures and various treatment times.

The results show that the mechanism of plastic yielding can lead to complete densification of the tablet when the pressure and the temperature are sufficiently high. This finding is very apparent in the case of superalloy metal

ISSN: 2319-5967
ISO 9001:2008 Certified
International Journal of Engineering Science and Innovative Technology (IJESIT)
Volume 4, Issue 3, May 2015

powders and tool steel. On the other hand, in the case of the alumina powder, the contribution of the mechanism of plastic yielding is practically negligible. This is related to the very high mechanical properties of the base material of these powders with a yield stress around 2100 MPa at ambient temperature.

The densification mechanism of plastic yielding causes a broadening of contacts between particles allowing densification to proceed when it is not complete. Mechanisms may be involved in the process of densification after plastic yielding are creep and mass transfer by diffusion.

Power law creep is a process of time-dependent deformation that causes a flow of material from contacts to the free surfaces of the particles. Apart from the diagrams corresponding to the alumina powder, the field of dominance of this mechanism appears in all other diagrams densification of the powders that we studied. In addition, this area is often much larger than those of other mechanisms. This shows that, in most cases, the mechanism of power law creep is the one that contributes the most to the densification of a powder aggregate when the plastic flow does not cause the total densification of the tablet.

Mechanisms of mass transfer by diffusion are very slow. Their contributions to the densification of the powders investigated are significantly lower than those of deformation mechanisms. The mechanism of grain boundary diffusion becomes dominant when the treatment temperature is higher and the applied pressure is too low to cause the flow of material by plastic deformation or creep. This situation occurs in the case of alumina powder where is observed that the total densification is achieved by boundary diffusion mechanism in a wide range of pressures and temperatures. The results also show that the contribution to densification of the lattice diffusion from the grain boundaries mechanism is not significant. The domain of preponderance of this mechanism appears on any maps densification that we have established. It should be noted that the mechanisms of material transport play an important role in the consolidation of the final product by increasing its toughness.

The Nabarro-Herring/Coble creep mechanism consistently contributes to the densification of the powder of special steels and super alloys. This mechanism is activated when the grain size is much smaller than that of the powder particles as in the case of super alloy and high alloy steels.

## VII. CONCLUSION

The simulations were performed for powders based on materials chosen for their very different mechanical characteristics. We have developed a new approach that allows correcting some short comings in earlier models. To simulate the HIP densification of the various studied powders, we have recalculated the expressions of coordination number, average contact area, and effective pressure. The new expressions obtained were used to establish the equations of densification mechanisms.

The simulations were performed by summing the contributions of the different mechanisms of plastic yielding, creep, and material flow associated with the lattice and grain boundaries diffusions.

The simulation results were compared with experimental data from literature. The theoretical predictions are close to the experimental values, we could then prepare the maps densification by hot isostatic pressing of the powders investigated. The method can be extended to other powders and the information obtained may be used for industrial applications.

As prospects in this regard, we plan to interest to the densification process during the rise HIP cycles. We can then take into account this part in simulations and certainly improve the theoretical results.

## REFERENCES

[1] E. Arzt, M. F. Ashby, and K. E. Easterling, “Practical applications of Hot Isostatic Pressing Diagrams: Four case studies,” Metall Trans A, vol. 14A, pp. 211-220, 1983.

[2] F. B. Swinkels, D. S. Wilkinson, E. Arzt, and M. F. Ashby, “Mechanisms of hot isostatic pressing,” Acta Metall, vol. 31, pp. 1829-1840, 1983.

[3] A. S. Helle, K. E. Easterling, and M. F. Ashby, “Hot isostatic pressing diagrams: new developments,” Acta Metall, vol. 33(12), pp. 2163-2174, 1985.

ISSN: 2319-5967
ISO 9001:2008 Certified
International Journal of Engineering Science and Innovative Technology (IJESIT)
Volume 4, Issue 3, May 2015

[4] E. Arzt, "The influence of an increasing particle coordination on the densification of spherical powders," Acta Metall, vol. 30, pp. 1883-1890, 1982.

[5] L. Redouani and S. Boudrahem, "Hot isostatic pressing process simulation: application to metal powders," Can J Phys, vol. 90, pp. 573-583, 2012.

[6] S. Boudrahem and M. Grosbras, "Evolution de la morphologie des pores durant la compression isostatique à chaud de poudres sphériques," Mater Tech, vol. 9-10, pp. 21-24, 1999.

[7] G. D. Scott, "Radial distribution of the random close packing of equal spheres," Nature, vol. 194, pp. 956-957, 1962.

[8] G. Mason, "Radial distribution functions from small packing of spheres," Nature, vol. 217, pp. 733-735, 1968.

[9] D. S. Wilkinson and M. F. Ashby, "Pressure sintering by power law creep," Acta Metall, vol. 23, pp. 1277-1285, 1975.

[10] M. F. Ashby, "Background reading HIP 6.0: Sintering and isostatic pressing diagrams," Engineering Department Trumpington, Cambridge University, 1990.

[11] H. J. Frost, M. F. Ashby, "Deformation-mechanism maps, the plasticity and creep of metals and ceramics," Pergamon Press, Oxford, 1982.

## APPENDIX

The laws of variation of the yield strength and the shear modulus of the base-materials of powders of the according to the temperature are given respectively by:

$\sigma_y = \sigma_{y0}\{1+\alpha[(T-300)/T_m]\}$ with $\alpha = (T_m/\sigma_{y0})(d\sigma_y/dT)$

$\mu = \mu_0\{1+\beta[(T-300)/T_m]\}$ with $\beta = (T_m/\mu_0)(d\mu/dT)$

and those of grain boundary diffusion coefficient, lattice diffusion, and power law creep constant are given respectively by:

$D_b = D_{0b}\exp(-Q_b/R_gT)$

$D_v = D_{0v}\exp(-Q_v/R_gT)$

## SYMBOLS AND UNITS

$A$ steady-state power-law creep constant
$A'$ Dorn's constant
$a$ average contact area ($m^2$)
$b$ Burger's vector (m)
$C$ slope of the radial distribution function of RDP
$D$ relativedensity
$\dot{D}$ relative density rate
$D_0$ initial relative density
$D_{0b}$ grain boundary auto-diffusion coefficient ($m^2s^{-1}$)
$D_{0v}$ lattice auto-diffusion coefficient ($m^2s^{-1}$)
$D_b$ grain boundary diffusion coefficient ($m^2s^{-1}$)
$D_v$ lattice diffusion coefficient ($m^2s^{-1}$)
$D_y$ relative density from yielding
$\overline{G}$ Average grain size (m)
$g(D)$ function of $D$
$k$ Boltzmann's constant ($JK^{-1}$)
$n$ steady-state power-law creep exponent
$P$ external pressure ($Nm^{-2}$)
$P_{eff}$ effective pressure ($Nm^{-2}$)
$P_{lim}$ limiting pressure causing yielding ($Nm^{-2}$)
$Q_v$ activation energy of lattice diffusion ($Jmol^{-1}$)
$Q_b$ activation energy of boundary diffusion ($Jmol^{-1}$)
$r_p$ pores radius during final stage(m)
$R$ average radius of particles (m)
$R_g$ perfect gases constant ($JK^{-1}mol^{-1}$)
$R'$ particle radius after densification (m)

ISSN: 2319-5967
ISO 9001:2008 Certified
International Journal of Engineering Science and Innovative Technology (IJESIT)
Volume 4, Issue 3, May 2015

$T$ treatment temperature (K)
$T_m$ melting temperature (K)
$x$ neck radius (m)
$Z$ average number of contacts per particle
$Z_0$ initial number of contacts per particle
$\alpha$ Dépendance de la limite élastique en fonction de la température
$\beta$ Dépendance du coefficient de cisaillement en fonction de la température
$\Delta t$ Incrémentation de temps (s)
$\delta$ Boundary thickness (m)
$\dot{\varepsilon}$ Deformation rate ($s^{-1}$)
$\dot{\varepsilon}_0$ Deformation rate at ambient temperature ($s^{-1}$)
$\Omega$ atomic volume ($m^3$)
$\sigma$ stress ($Nm^{-2}$)
$\sigma_0$ yield stress at 300 K ($Nm^{-2}$)
$\sigma_y$ yield stress ($Nm^{-2}$)
$\mu$ shear modulus ($Nm^{-2}$)
$\mu_0$ shear modulus at 300 K ($Nm^{-2}$)